Journal of Applied Mechanical Engineering
ISSN: 2168-9873

Kawabata et al., J Appl Mech Eng 2018, 7:4
DOI: 10.4172/2168-9873.1000309

Research Article Open Access

# Development of Wind in Flow Measurement System Using 9-Beam Nacelle Lidar

**Hirokazu Kawabata*, Yoshihiro Kikushima and Tetsuya Kogaki**

*Fukushima Renewable Energy Institute, National Institute of Advance Industrial Science and Technology (AIST), Machiikedai, Koriyama, Fukushima, Japan*

## Abstract

This paper reports on wind inflow measurements performed using a nine-beam nacelle lidar. Various nacelle lidar systems have been used for the measurements of wind inflow to realize high-performance wind turbines. The measurement of a two-beam nacelle lidar used as a simple measurement system has been compared with those of a nacelle anemometer and a met-mast. The 10-min-averaged data obtained from the two-beam nacelle lidar have good measurement accuracy, but the lidar is unable to measure wind shear. Monitoring of wind in-flow for multi-megawatt wind turbines requires an advanced lidar system that can measure wind shear. Further, there is a lack of observation reports on measurements using the two-beam nacelle lidar under strong turbulence conditions. In this study, the authors evaluated the measurement characteristics of a nine-beam nacelle lidar installed on a 300-kW wind turbine. This nacelle lidar could measure radial wind speeds in nine directions; further, horizontal wind speeds were measured using a three-beam system. The use of three beams led to a considerably higher availability of the lidar in comparison to the availability when using two beams. This lidar also could measure wind speed uniformity in a transverse direction by using three beams. To discriminate the lidar measurement data in terms of their quality, some filtering indexes for these data were proposed. Continuous and reliable monitoring of wind shear could be achieved by filtering the measured data.

**Keywords:** Wind turbine; Nacelle lidar; Wind measurement; Remote sensing

## Introduction

Generally, nacelle anemometer is used for wind monitoring and machine control during wind turbine operation. The problem with using nacelle anemometer is that the sensor is affected by the wake of the turbine blades, which hinders accurate measurement of wind inflow information which affects the power generation. Therefore, there has been a growing interest in the development of an approach for solving these problems. A nacelle lidar, which is a measurement instrument for observing wind inflow, is useful in realizing wind monitoring not affected by wake. The instrument emits a stream of photons that interact with a variety of particulates in the air, some of which is scattered back toward the lidar where the signal is analyzed, and wind data is reported based on the doppler shift phenomenon [1]. As an alternative to the nacelle anemometer, the nacelle lidar can be a useful wind sensor for wind turbine operation. Previous research has suggested that a nacelle lidar reduces the mean cost of energy in some application [2].

A number of studies have been conducted on pulsed and continuous-wave (CW) nacelle lidar. The CW lidar has a short measurable range (from 10 m to a few hundred meters) and can be used to obtain measurements in a single range. A circular scan CW lidar was successfully used to measure vertical wind shears [3-6]. Furthermore, a good agreement was observed between the wind speed and wind direction data measured using a circular scan lidar and the corresponding data measured using a met mast near the hub height.

In contrast, the pulsed lidar has a wide observation range (from 40 m to 2.000 m), and it can be used for the simultaneous measurement of more than 10 ranges. Because of these advantages, the authors have been developing a wind turbine system utilizing pulsed nacelle lidar. Studies on a simple two-beam type pulsed lidar are typical and representative. Wind inflow data measured using a two-beam nacelle lidar have been compared with those measured using a met mast [7-9]. In these studies, both the sets of wind inflow data showed a strong positive linear correlation. In the case that the wind speeds were higher than the cut-in wind speed, the measurement uncertainty in the horizontal wind speeds obtained using a nacelle lidar was reported to be 0.88% to 1.8% [10]. The results of field tests performed using a nacelle lidar demonstrated that the lidar improved the power capture significantly in comparison to a nacelle anemometer [11]. However, the two-beam nacelle lidar, which is a simple and inexpensive instrument, cannot be used to measure wind shear. In particular, the wind shear of wind inflow has an impact on large-scale wind turbines.

In the present study, the authors measured wind inflow by using a pulsed nine-beam nacelle lidar. This lidar has an advantage in that it can measure horizontal and vertical wind shears in more than one area by the use of nine beams. The purpose of this study was to investigate the measurement characteristics of the nine-beam nacelle lidar. Wind in-flow data measured by the nine-beam nacelle lidar were compared with those measured by a nacelle anemometer. This paper presents the results of measurements performed over a 1-month period.

## Experimental Setup

### Test site and wind turbine

A field test was performed at the Fukushima Renewable Energy Institute, AIST (FREA). Figure 1a shows a map of the terrain around the test site. A range of approximately 2 km around the test site is almost flat terrain. The prevailing wind direction in this field is northwest,

***Corresponding author:** Kawabata H, Fukushima Renewable Energy Institute, National Institute of Advance Industrial Science and Technology (AIST), 2-2-9 Machiikedai, Koriyama, Fukushima 963-0298, Japan, Tel: +81-298613632; E-mail: kawabata-h@aist.go.jp

**Received** June 27, 2018; **Accepted** July 16, 2018; **Published** July 20, 2018

**Citation:** Kawabata H, Kikushima Y, Kogaki T (2018) Development of Wind in Flow Measurement System Using 9-Beam Nacelle Lidar. J Appl Mech Eng 7: 309. doi:10.4172/2168-9873.1000309

and a mountainous area lies at a distance of 2 km from the field. The strong wind mainly blows from the northwest, and nonuniform wind conditions were sometimes expected. The difference in altitude between the test site and the mountaintop is approximately 800 m. A Komaihaltec 300-kW up-wind type wind turbine (KWT300) situated in the test field was used for this study. The wind turbine is resistant to mountain winds with its turbulence parameter set above the IEC class IIA standard. The specifications of the wind turbine are listed in Table 1. A met mast of a height of 20 m is located at a distance of 83 m from the wind turbine. Figure 1b shows the relationship between wind speeds and turbulence intensities measured using the met mast. The red plots indicate the bin-averaged measurements, and the blue plots represent the 90 percentiles. The specifications of the cup and vane anemometers (Adolf Thies GmbH & Co. KG) installed on the met mast and nacelle are listed in Table 2. The field tests were performed in May 2015.

## Setup of Nacelle lidar

A prototype of the Mitsubishi Electric nine-beam nacelle lidar system was used for the present study. This nacelle lidar can be used to measure radial wind speeds in nine lines of sight (LOS0–LOS8), as shown in Figure 2a. The optical head of the lidar was considered as the origin, and the LOS0 beam was considered as the x-axis. The main idea of the nine-beam nacelle lidar is to measure wind inflow at a high resolution. The beams were switched in the order of LOS3, LOS2, LOS1, LOS5, LOS0, LOS4, LOS8, LOS7, and LOS6. Radial wind speeds were measured in 20 ranges (-300 m ≤ x ≤ -62.5 m, -9.1 ≤ x/D ≤ -1.9) simultaneously. The probed length per range was 25 m, and each probe region was half overlapped. Compared to nacelle anemometer, the lidar detects the averaged wind speed component within the large measurement volumes. The horizontal and vertical cone angles (Figures 2b and 2c) were $\theta_1$=15° and $\theta_2$=10°, respectively. In order to prevent the beam from hitting the ground near the wind turbine, θ2 was set to be smaller than θ1. It should be noted that the beams in the lower row hit the ground at x/D = -6.7. The specifications of the nacelle lidar are listed in Table 3.

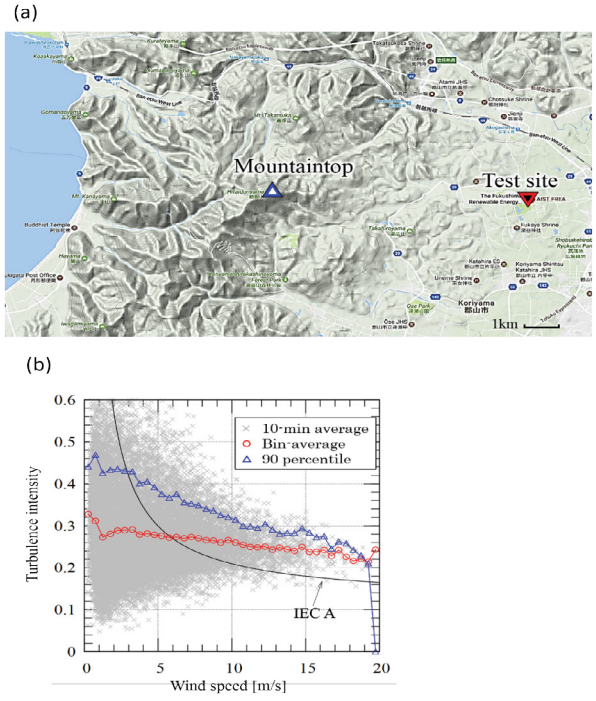


**Figure 1 (a):** Map of terrain around the test site, **(b)** Turbulence intensity distribution.

The longitudinal and transversal wind speed components $V_x$ and $V_y$, respectively, were measured for the three rows (upper, middle, and lower). Figure 3a shows a reference example of the method of wind speed calculation in the middle row. Typically, Doppler lidar can only be used to measure the wind speeds in the direction of the laser beams' directions. The radial wind speeds $v_3$ and $v_4$ are expressed in Equation 1, and the wind speed components for each measurement position can be written as shown in Equation 2.

$$v_4 = V_{x,4}\sin\theta_1 + V_{y,4}\cos\theta_1 \quad (1)$$

$$v_5 = V_{x,5}\sin\theta_1 - V_{y,5}\cos\theta_1 \quad (2)$$

In order to calculate the wind speed components using the radial speeds $v_4$ and $v_5$, it must be assumed that the horizon-tal wind is uniform in the measurement volume during the measurement (Figure 3, green vectors). If the horizontal wind uniformity in temporal and special is assumed by Equation 3, the wind speed components can be predicted using Equation 4. This is the same measurement principle as that used for a two-beam nacelle lidar.

$$V_{x,4} = V_{x,5} = V_{x,mid}, \qquad V_{y,4} = V_{y,5} = V_{y,mid} \quad (3)$$

$$V_{x,mid} = \frac{v_4 + v_5}{2\cos\theta_1}, \qquad V_{y,mid} = \frac{v_5 - v_4}{2\sin\theta_1} \quad (4)$$

The wind speed components for the upper and lower row can be calculated in a manner similar to the calculation of the middle row. It should be noted that $V_x$ for the upper and lower rows was corrected using the cone angle $\theta_2$. As a result, it was possible to measure the vertical wind shear.

| | |
|---|---|
| Rated power | 300 kW |
| Cut-in wind speed | 3.0 m/s |
| Cut-out wind speed | 25 m/s |
| Survival wind speed | 70 m/s |
| Turbine diameter (*D*) | 33 m |
| Hub height | 41.5 m |

**Table 1:** Specifications of the wind turbine.

| Variables | Accuracy | Sampling rate |
|---|---|---|
| Cup anemometer | 1% of measurement value or <0.2 m/s | 1 Hz |
| Vane anemometer | 1° | 1 Hz |

**Table 2:** Key specifications of nacelle anemometers.

| | |
|---|---|
| Laser wavelength | 1550 nm |
| Number of ranges | 20 |
| Probe length | 25 m |
| Probe overlap rate | 50% (= 25 m) |
| Position of minimum range | 62.5 m (center of the probe) |
| Measured range of radial wind speed | 40 m/s to -20 m/s (plus: headwind) |
| Measurement accuracy of radial wind speed | 0.1 m/s |
| Sampling rate of radial wind speed | 4 Hz |

**Table 3:** Specifications of nacelle lidar.

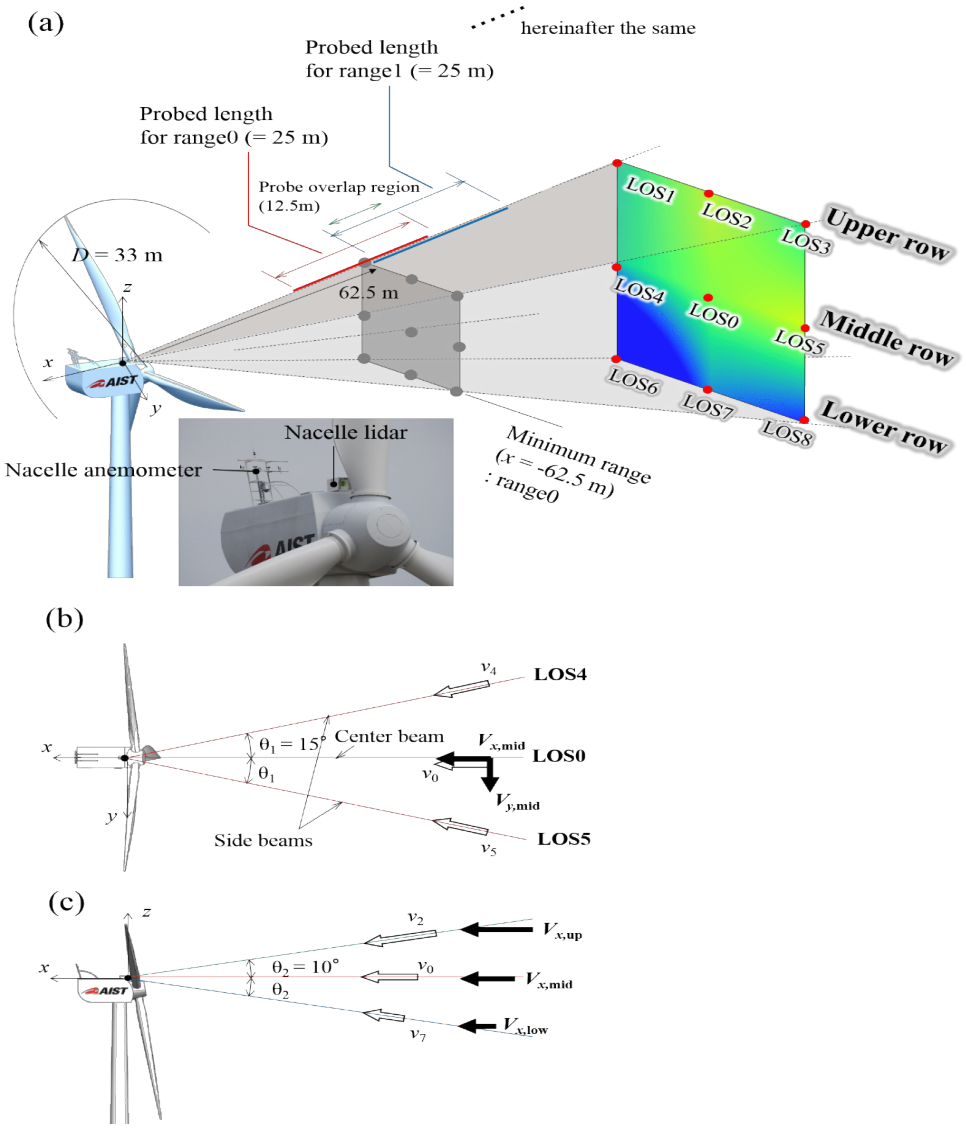


**Figure 2:** Setup outline of the nine-beam nacelle lidar: (a) Perspective view, (b) Top view, (c) Side view.

$$V_{x,up} = \frac{v_1 + v_3}{2\cos\theta_1 \cos\theta_2}, \qquad V_{x,low} = \frac{v_6 + v_8}{2\cos\theta_1 \cos\theta_2} \tag{5}$$

$$V_{y,up} = \frac{v_3 - v_1}{2\sin\theta_1}, \qquad V_{y,low} = \frac{v_8 - v_6}{2\sin\theta_1} \tag{6}$$

The nine-beam lidar was used to measure the longitudinal wind speed component directly as radial wind speeds of the three center beams: LOS2, LOS0, and LOS7 (Figure 4). The assumption in Equation 3 is not necessary to obtain this measurement.

$$V_{x,up} = \frac{v_2}{\cos\theta_2}, \qquad V_{x,mid} = v_0, \qquad V_{x,low} = \frac{v_7}{\cos\theta_2} \tag{7}$$

If the temporal and spatial horizontal wind uniformity can be assumed, the value of $V_x$ directly measured by the center beam and that predicted from the two radial wind speeds obtained by the side beams should be equal. The center beams are unprecedented devices for evaluating the horizontal wind uniformity.

$$\Delta V_x = \left| V_{x,center-beam} - V_{x,side-beam} \right| \approx 0 \tag{8}$$

The horizontal wind speed V for each row was derived as given in Equation 9:

$$V = \sqrt{V_x^2 + V_y^2} \tag{9}$$

Each of the averaged wind speeds was calculated using Equation 10, where n is the number of elements in each averaging time.

$$\bar{u} = \frac{1}{n}\sum_{i=1}^{n} u_i \tag{10}$$

The turbulence intensity TI can be expressed using the mean and standard deviation of the averaged wind speeds as follows:

$$T = \frac{1}{\bar{u}}\sqrt{\frac{1}{n}\sum_{i=1}^{n}\left(u_i - \bar{u}\right)^2} \tag{11}$$

Figure 4 shows the measurement system with time for the nine-beam nacelle lidar. This figure shows the measurement method for the middle row; the same method was also used for the other two rows. Nine radial wind speeds were measured in turn. The circles indicate the

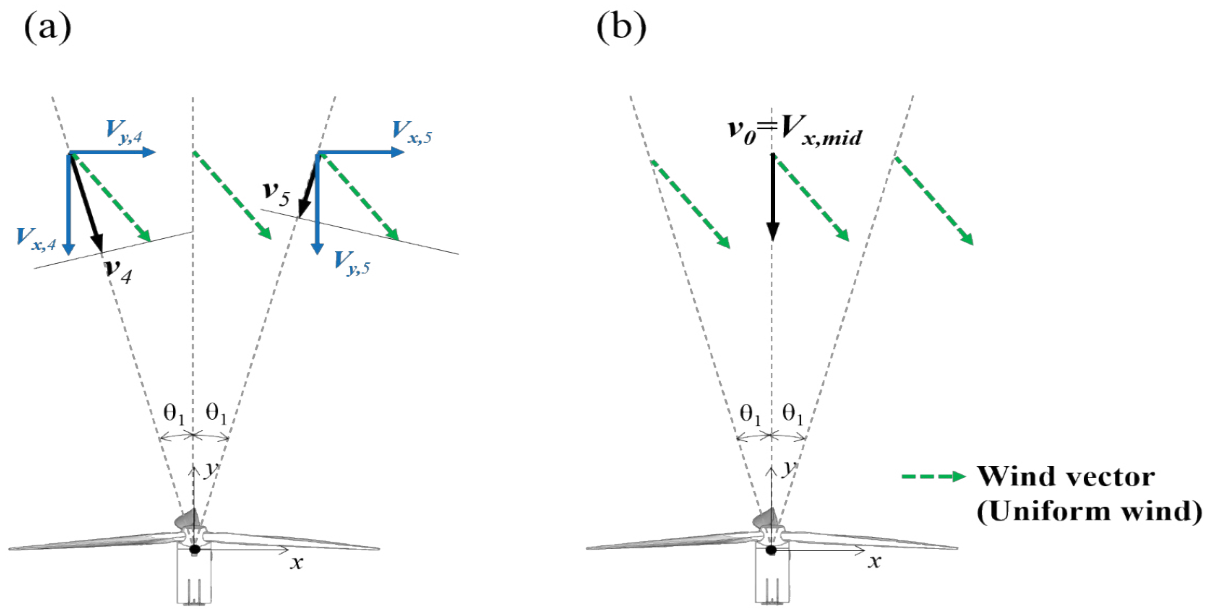


**Figure 3:** Calculation method for wind speed components: (a) Two-beam measurement, (b) Center beam measurement.

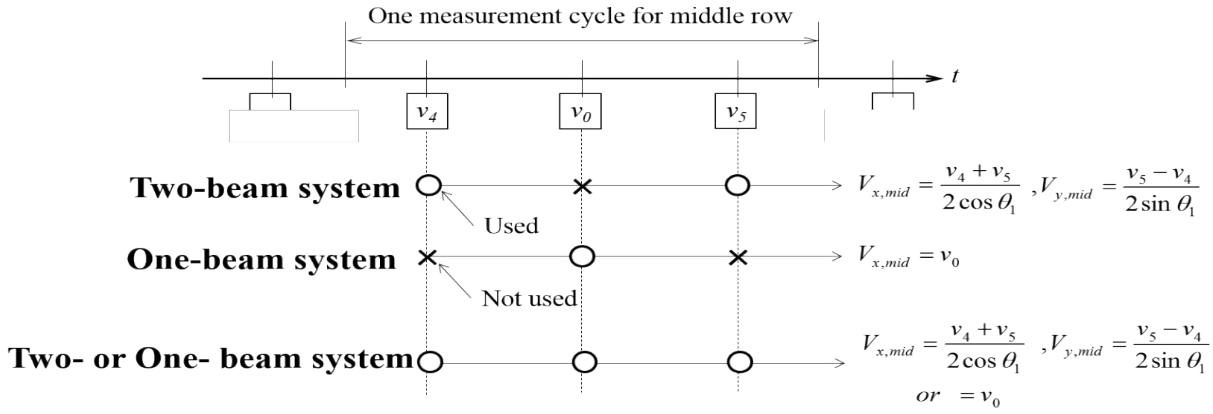


**Figure 4:** Measurement system for longitudinal wind speed component using middle row of the nine-beam nacelle lidar.

data used to calculate the wind speed components, and the cross marks indicate the data that was not used for the calculation. The two-beam system is a conventional system in which the longitudinal wind speed component is calculated using the left and right beams. The temporal and spatial wind uniformity was assumed during the one-measurement cycle. A beam sometimes hits the turbine blades, and these results in the loss of the measurement signals. If the measurement signal of $v_4$ or $v_5$ was not obtained, $V_{x,mid}$ could not be calculated. The one-beam system directly measures the longitudinal wind speed component using only the center beam. The nine-beam lidar combines the two systems to improve the data availability and verify the wind uniformity. Even if the measurement signal could not be obtained with the two-beam system, the signal obtained from the center beam was used for the wind speed calculation.

## Results and Discussion

### Lidar availability

Often, it is not possible to obtain measurement signals using lidar unlike in the case of a cup anemometer. The collision of the beams with the turbine blades and the deficiency of the aerosol makes it difficult to obtain measurement signals. Lidar availability is defined as the percentage of the number of data samples for which wind speed signals were obtained in the measurement time (Equation 12). $n_{total}$ is the total number of measurements, and $n_{available}$ is the total number of obtained measurement signals in a unit of time (10 min).

$$Availability = \frac{n_{available}}{n_{total}} \quad (12)$$

A high availability results in a superior statistical reliability of the measurements. Therefore, the evaluation of the lidar availability is an important task. Figure 5 shows the relationship between the 10-min-averaged lidar availability of a one-beam system, turbine rotor speed, and radial wind speed. As the availability of the measurements was similar for all the beams, the availability of LOS0 was considered as the representative case. The plots of were colored by Vx,mid measured using the nacelle lidar at x/D = -2.3. The square plots indicate the bin-averaged (2 m/s bin) availability. The nacelle lidar is required to

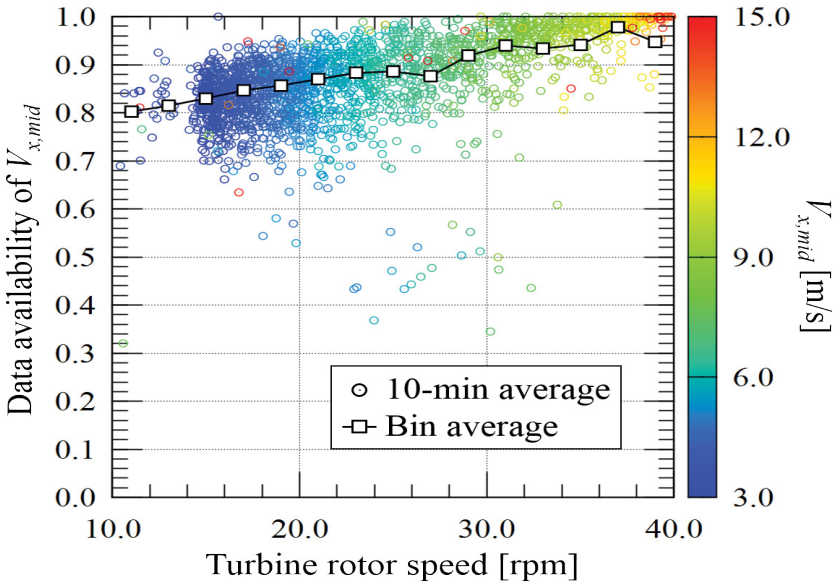


**Figure 5:** Relationship between 10-min-averaged availability of radial wind speed (LOS0, x/D = -2.3) and turbine rotor speed.

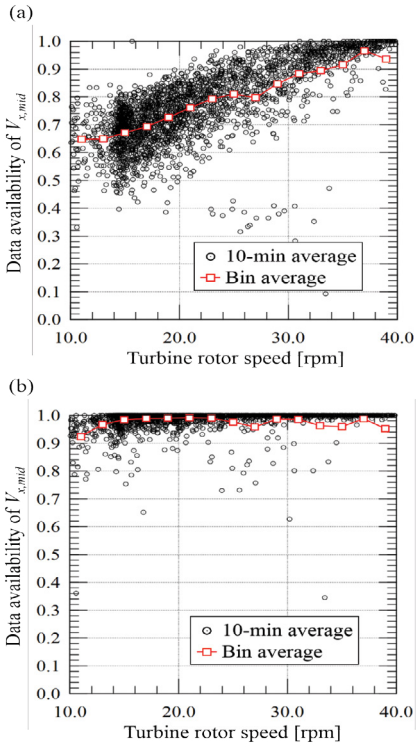


**Figure 6:** Relationship between the 10-min-averaged availability of $V_{x,mid}$ (middle row, x/D = -2.3) and turbine rotor speed: **(a)** Two-beam system, **(b)** One- or two-beam system.

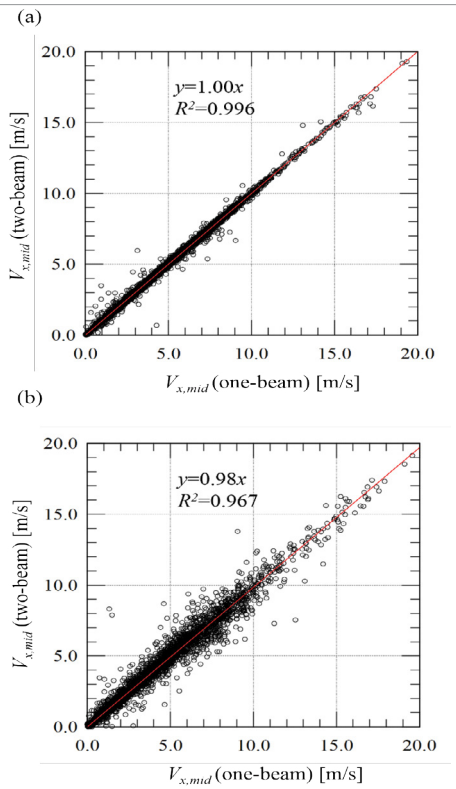


**Figure 7:** Ten-min-averaged $V_{x,mid}$ measured using one- and two-beam systems in two range: **(a)** Range ( x/D = -1.9) , **(b)** Range 10 (x/D = -5.7).

measure the power curve instead of the met mast specified in the IEC standard. The measured range is the closest to x/D = -2.5. During the operation of the wind turbine (at approximately 10 to 40 rpm), the availability was the lowest in around the cut-in wind speed. In the case of a very low rotor speed, the time for one blade cover the nacelle lidar was long against signal detection time for radial wind speed (about 0.25 s). As the rotor speed was in-ceased, the availability increased continuously. Fast rotor speeds reduce the covered time per one blade, and many pulses passed through the blade within one measurement time. The bin-averaged availability exceeded approximately 0.8 for almost all the wind speeds.

Figure 6a shows the availability of $V_{x,mid}$ data obtained using the two-beam system. The black plots indicate the 10-min-averaged availability, and the square plots indicate the bin-averaged (2 m/s bin) availability. The availability of the two-beam system had exhibited a trend similar to that of the one-beam system, but the bin-averaged values of the availability were relatively low. The determination of measurement success for this system was more severe than one-beam system, because it required measurement signals for both the left and right beams in order to calculate the wind speed. Figure 6b shows the availability of $V_{x,mid}$ data obtained using the one- or two-beam system. In the case of this system, the availability did not depend on the rotor speed. Even if data loss occurred in the one-beam system, the other system provided the data of $V_x$. Therefore, the probability of obtaining the measurement signal was high, and these measurements suggest that the center beam can contribute to the increase in the $V_x$ data availability and the reliability of the statistical data.

## Comparison of one- and two-beam measurement systems

As previously stated, for the wind-speed calculation method using two radial wind speeds, the temporal and spatial horizontal wind uniformity is assumed. However, the information regarding the wind uniformity cannot be confirmed using conventional nacelle lidar. This section presents the evaluation of the horizontal wind uniformity using three beams. While the two-beam system requires temporal and spatial homogeneity in the measurement principle, the one-beam system can be used to directly measure the wind speed component. If the spatial wind uniformity is assumed in the measurement period, the measured Vx obtained using the one-beam and two-beam systems should be equal (Equation 8). Figures 7a and 7b show a comparison of the 10-min-averaged $V_{x,mid}$ data in the middle row as measured using the one- and two-beam systems. The red lines represent the approximate line calculated using the least-squares method. In range 0, the small wind speed differences indicate that the wind uniformity was sufficiently secured in several cases. In the measurement range far from that of the nacelle lidar, the distance between the left and right beams and the center beam was great. In range 10, the left and right beams were approximately 110 m apart. As the spread of the left and right beams is large, the corresponding measurements were influenced by the spatial wind nonuniformity as compared to those for range 0. Although linearity was observed, a difference of 3 to 5 m/s was sometimes obtained between the $V_x$ estimated using the two-beam system and the directly measured $V_x$.

## Comparison of wind speed measurements obtained using lidar and nacelle anemometer

In this study, the wind inflow data measured using the nine-beam nacelle lidar were compared with those measured using a reference anemometer. A nacelle anemometer is commonly used for feedforward control and power performance verification. As the met mast in the test field was shorter than the hub height of the wind turbine, the nacelle anemometer was chosen as the reference anemometer.

Figure 8 shows a comparison of 10-min-averaged wind speeds, wind directions, and turbulence intensities measured using the nacelle anemometer and the nine-beam nacelle lidar at x/D = -1.9. The averaging time for the nacelle lidar and the nacelle anemometer measurements were the same. A time delay occurs until the inflow measured by the nacelle lidar arrives at the nacelle. In order to minimize the influence of the time delay in the statistics, the nearest measurement range for the nacelle and 10-min-averaged measurements were evaluated. The black plots (filtered data: 678 samples) show that the 10-min-averaged availability exceeds 70% and $\Delta Vx/Vx < 0.1$ in the raw data. The gray plots did not satisfy the filtering conditions. Figure 8a shows a comparison of the wind speeds measured using the nine-beam nacelle lidar and the nacelle anemometer. The line of the approximate values was calculated using the least-squares method, and its slope exceeded 1.0 owing to the deceleration of the turbine rotor. By using the filter, much of the data with low availability at low wind speeds, as shown in Figure 6, were excluded. However, the use of the filter did not change the correlation as much as measurement data of turbulence intensity described later.

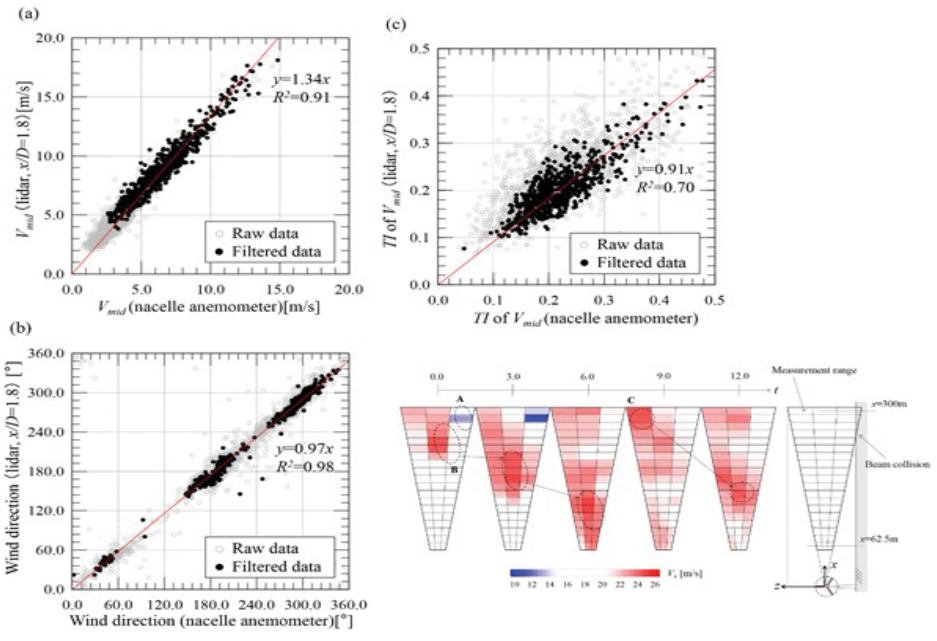


**Figure 8:** Comparison of three 10-min-averaged wind statistics obtained using the nacelle anemometer and nine-beam nacelle lidar (middle row, x/D = -1.9): **(a)** Horizontal wind speed, **(b)** Wind direction, **(c)** Turbulence intensity.

The filtered data for the wind direction had a high correlation, which was similar to that of the wind speed. The low availability caused a large separation of the measurements from the fitted line, which was not observed in the wind speed data. The turbulence intensities measured using the nacelle lidar and nacelle anemometer showed a low correlation (Figure 8c). The variation in the turbulence intensity was greater than that in the wind speed and direction. In principle, wind speeds can be detected within a larger volume with a doppler lidar than that with a nacelle anemometer. The scale difference of the measured volume may have influenced the turbulence flow measurement.

### Vertical wind shear measurement

The nine-beam nacelle lidar can measure wind shear, and this measurement is required particularly for large wind turbines. The measurement cycle time of nine beams is about 3 s, which is relatively larger than that of the two-beam nacelle lidar. In this section, it is shown that the nine-beam nacelle lidar could measure a wind gust with the measurement cycle time.

Figure 8 shows the time series of longitudinal wind speed component contours obtained by the three-beam system in every measurement cycle. The wind speed contours are aligned with the measurement geometry. Measurement errors occurred at the collision location of the lower-row beams, in which low wind speeds were observed (see the dotted circle A). The dotted circles B and C indicate wind gusts. Despite the low measurement time resolution of the nine-beam nacelle lidar, the wind shear and the advection of the wind gust were clearly observed. The high lidar availability of the three-beam system compensated for the low time resolution, which was inevitably caused by the wind shear measurements. This measurement is particularly effective on condition monitoring of multi-megawatt wind turbines.

## Conclusions

In the present study, wind speeds were measured with the aim of understanding the measurement characteristics of a nine-beam nacelle lidar installed on a 300-kW wind turbine over a 1-month period. The following conclusions could be drawn on the basis of the study findings.

1. When the three-beam system was used for $V_x$ measurement, the lidar availability for $V_x$ data was higher than that of the two-beam system. This improved lidar availability is attributed to the center beam in the three-beam system. Since the 9-beam nacelle lidar can measure wind shear, high availability is effective for wind monitoring during continuous wind turbine operation.
2. The wind speed and direction measured by the nine-beam nacelle lidar had a high correlation with those measured by the nacelle anemometer. As an alternative to nacelle anemometer, the nacelle lidar may be used for wind monitoring during turbine operation. However, the turbulence intensity was significantly affected by the differences in measurement instruments, which led to a low correlation between the turbulence intensities measured by the nacelle lidar and the nacelle anemometer.
3. In order to ensure reliability of statistical data, it is possible to filter data using availability and $\Delta V_x$. Data filtering processes were able to eliminate data not following the measurement principle. However, the filtering process caused a reduction in the amount of lidar data. Since the effect of filtering depends on the turbulence condition, the discovery of the optimum data filtering method is a future task.

In this study, wind inflow data were compared between the nacelle anemometer and the nine-beam nacelle lidar. Since the nacelle anemometer was affected by the wake of the turbine blades, the effect of the wake had to be excluded. New measurement instruments will be introduced in the future to eliminate the effects of the wake.

### Acknowledgments

The authors would like to thank Mitsubishi Electric Corporation for their assistance in providing technical support for the operation of the nine-beam nacelle lidar. The authors are grateful to Mami Okada for the setting up and operation of the measurement instruments.

### References

1. Lindelow P, Petter PR, Jacob J, Christensen T, Lintz E, et al. (2007) Fiber based coherent lidars for remote wind sensing.
2. Byrne A, McCoy TB, Rogers T (2012) Expected impacts on cost of energy through lidar based wind turbine control. Proceedings of EWEA Conference, Copenhagen, Denmark.
3. Pettenmeir A, Schlipf D, Würth I, Cheng PW (2014) Power performance measurements of the NREL CART-2 wind turbine using a nacelle-based lidar scanner. ℐ Atmospheric Ocean Technol 31: 2029-2034.
4. Smith M, Harris M, Medley J, Slinger C (2014) Necessity is the mother of invention: Nacelle-mounted lidar for measurement of turbine performance, Energy Procedia 53: 3-22.
5. Feeney S, Derrick A, Oram A, Campbell I, Hutton G, et al. (2014) Project cyclops: The way forward in power curve measurements, Europe's Premier Wind Energy Event.
6. Medley J, Slinger C, Barker W, Harris M, Pitter M, et al. (2014) Evaluation of wind flow with a nacelle-mounted continuous-wave lidar, Europe's Premier Wind Energy Event.
7. Wagner R, Courtney M, Pedersen TR, Gottschall J, Antoniou I, et al. (2013) Power performance measured using a nacelle-mounted lidar. DEWI Magazine 43: 49-55.
8. Wagner R, Davoust S (2013) Nacelle lidar for power curve measurement Avedøre campaign, DTU Vindenergi Report 2013.
9. Wagner R, Pedersen TF, Courtney M, Antoniou I, Davoust S, et al. (2014) Power curve measurement with a nacelle mounted lidar. Wind Energy 17: 1441-1453.
10. Wagner R, Courtney MS, Pedersen, Troels F, Davoust, S (2015) Uncertainty of power curve measurement with a two-beam nacelle-mounted lidar. Wiley Online Library 19: 1269-1287.
11. Fleming PA, Scholbrock AK, Jehu A, Davoust S, Osler E, et al. (2014) Field-test result using a nacelle-mounted lidar for improving wind turbine power capture by reducing yaw misalignment. ℐ Phys Conf Ser 524: 012002.